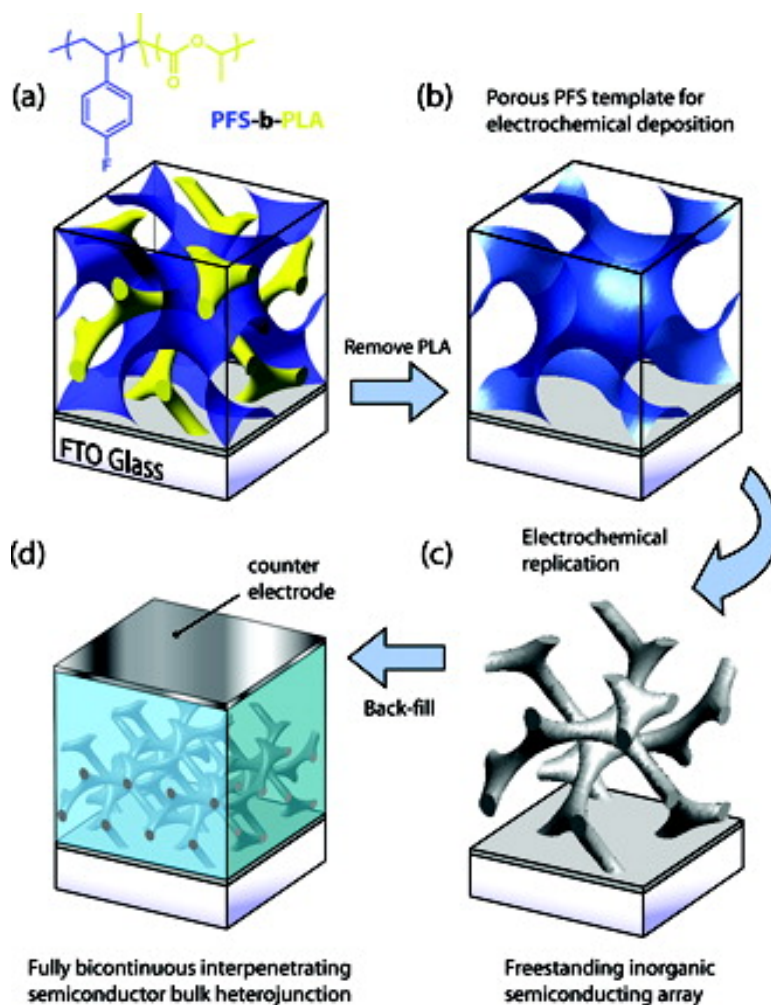# NANOLETTERS

Letter

A Bicontinuous Double Gyroid Hybrid Solar Cell

Edward J. W. Crossland, Marleen Kamperman, Mihaela Nedelcu, Caterina
Ducati, Ulrich Wiesner, Detlef -M. Smilgies, Gilman E. S. Toombes,
Marc A. Hillmyer, Sabine Ludwigs, Ullrich Steiner, and Henry J. Snaith

More About This Article

ACS Publications
High quality. High impact.

Additional resources and features associated with this article are available within the HTML version:

- Supporting Information
- Access to high resolution figures
- Links to articles and content related to this article
- Copyright permission to reproduce figures and/or text from this article

View the Full Text HTML

A Bicontinuous Double Gyroid Hybrid Solar Cell

Edward J. W. Crossland,[†,‡] Marleen Kamperman,[§] Mihaela Nedelcu,[†]
Caterina Ducati,[||] Ulrich Wiesner,[§] Detlef -M. Smilgies,[⊥] Gilman E. S. Toombes,[#]
Marc A. Hillmyer,[∇] Sabine Ludwigs,[†,○] Ullrich Steiner,[*,†] and Henry J. Snaith[*,◆]

*Department of Physics, Cavendish Laboratory, University of Cambridge,
Cambridge CB3 0HE, U.K., University of Cambridge Nanoscience Centre,
Cambridge, CB3 0FF, U.K., Freiburg Institute for Advanced Studies,
Albert-Ludwigs-Universität Freiburg, 79104 Freiburg, Germany, Department of
Materials Science & Engineering, Cornell University, Ithaca, New York 14853,
Department of Materials Science & Metallurgy, University of Cambridge, Cambridge,
CB2 3QZ, U.K., Cornell High Energy Synchrotron Source (CHESS), Cornell
University, Ithaca, New York 14853, Physical Chemistry—UMR CNRS 168, Institute
Curie, 11 rue Pierre et Marie Curie, 75005 Paris, France, Department of Chemistry,
University of Minnesota, Minneapolis, Minnesota 55455-0431, Institute for
Macromolecular Chemistry & Freiburg Materials Research Centre, University of
Freiburg, Stefan-Meier-Strasse 31, 79104 Freiburg, Germany, and Clarendon
Laboratory, Department of Physics, University of Oxford, OX1 3PU, U.K.*

ABSTRACT

We report the first successful application of an ordered bicontinuous gyroid semiconducting network in a hybrid bulk heterojunction solar cell. The freestanding gyroid network is fabricated by electrochemical deposition into the 10 nm wide voided channels of a self-assembled, selectively degradable block copolymer film. The highly ordered pore structure is ideal for uniform infiltration of an organic hole transporting material, and solid-state dye-sensitized solar cells only 400 nm thick exhibit up to 1.7% power conversion efficiency. This patterning technique can be readily extended to other promising heterojunction systems and is a major step toward realizing the full potential of self-assembly in the next generation of device technologies.

The conversion of light to electrical energy in solar cells that are based on organic or ceramic materials depends sensitively on the way these materials are arranged on the 10 nm length scale.[1,2] Hybrid composites, which are composed of organic and inorganic semiconductors and ceramics, can be fabricated from a broad range of materials and structured at a mesoscopic, nanoscopic, and molecular level. Correctly matching the materials and structure can deliver

exceptional electronic properties which can be exploited in a broad range of applications. The bulk heterojunction solar cell concept for example exploits an extremely fine yet continuous interdigitation of donor and acceptor material phases distributed throughout the thickness of the active layer to achieve efficient separation and extraction of free charges.[3–5]

The solid-state dye-sensitized solar cell (SDSC) is one of the most promising nanotechnology-based hybrid photovoltaic systems and has sparked widespread interest in fabricating mesoscopic semiconductor materials with very large internal surface areas.[6,7] For this type of solar cell light absorption takes place in a molecular sensitizer sandwiched between an n-type metal oxide and an organic hole transport material. Because light is harvested in a monolayer of dye, a large surface to volume ratio of the metal oxide is required to load the system with sufficient dye density for complete light absorption. Currently the best approach to forming mesoporous metal−oxide layers is by sol−gel processed sintered nanoparticles which produces a disordered, highly

* Corresponding authors, u.steiner@bss.phy.cam.ac.uk and h.snaith1@physics.ox.ac.uk.
† Department of Physics, Cavendish Laboratory, University of Cambridge, and University of Cambridge Nanoscience Centre.
‡ Freiburg Institute for Advanced Studies, Albert-Ludwigs-Universität Freiburg.
§ Department of Materials Science & Engineering, Cornell University.
|| Department of Materials Science & Metallurgy, University of Cambridge.
⊥ Cornell High energy Synchrotron Source (CHESS), Cornell University.
Physical Chemistry—UMR CNRS 168, Institute Curie.
∇ Department of Chemistry, University of Minnesota.
○ Institute for Macromolecular Chemistry & Freiburg Materials Research Centre, University of Freiburg.
◆ Clarendon Laboratory, Department of Physics, University of Oxford.

porous rough film. It is generally expected that a better control of the pore mesostructure will result in significant improvements in device performance and large area reproducibility for this class of solar cell.[2]

Material architectures defined by block-copolymer self-assembly are extremely promising candidates to improve hybrid device performance. The self-assembly of two dissimilar covalently bound polymer chains gives rise to the formation of extremely high internal area material junctions with periodicities on the 10 nm length scale.[8] While the introduction of functional materials into block-copolymer self-assemblies has been achieved in a number of ways,[9−13] after three decades of intensive study there remain very few examples of real functioning devices that exploit these fascinating self-assembled structures.[14,15]

Achieving continuous connectivity of all electronically active phases to the device electrodes is particularly challenging using block copolymers because most copolymer morphologies (e.g., columns or lamellae) usually exhibit only an in-plane continuity in thin films. This anisotropy in phase connectivity can be avoided by targeting the cubic bicontinuous double gyroid phase of diblock copolymers[16,17] in a selectively sacrificial system.[18,19] The double gyroid phase consists of two interwoven continuous networks of the minority polymer block held in a matrix phase of the majority block, which is centered on a gyroid surface (Figure 1a). The gyroid morphology has monodisperse pore diameters in which all channels and struts are fully interconnected. These attributes are conceptually ideal for the fabrication of hybrid solar cells where the open, uniformly sized pores enable effective infiltration of an organic phase and the predefined, monodisperse length scale enables optimized charge generation and collection through direct "nontortuous" pathways. Gyroid morphologies were recently reported in germanium[20] and have been replicated by platinum electrodeposition,[21] and ionic transport in one domain of the bicontinuous cubic morphology has been demonstrated.[22] However, to the best of our knowledge, the gyroid structure has never been exploited in a functioning electronic device of any type. Here, we report the replication of a metal−oxide semiconductor in the gyroid network phase via electrochemical deposition of anatase TiO_2 into a porous copolymer template, and the preparation of solid-state dye-sensitized solar cells with high power conversion efficiencies. The procedure is summarized schematically in Figure 1.

The diblock copolymer used in this study is poly(4-fluorostyrene)-b-poly(D,L-lactide) (PFS-b-PLA)[23] with a molecular weight of 36 kg mol^{-1} and containing $60\%_{mass}$ PFS. Small-angle X-ray scattering (SAXS) on an annealed bulk sample resulted in spectra that were consistent with a gyroid phase of unit cell length 49 nm (see Supporting Information). Thin films of PFS-b-PLA were prepared on conductive fluorine-doped tin oxide (FTO) glass substrates precoated with a ~50 nm thick compact layer of TiO_2 by spray pyrolysis deposition. The copolymer was annealed at 180 °C for 35 h, and after cooling to room temperature the PLA block was selectively etched by immersing the films in a mild aqueous base.
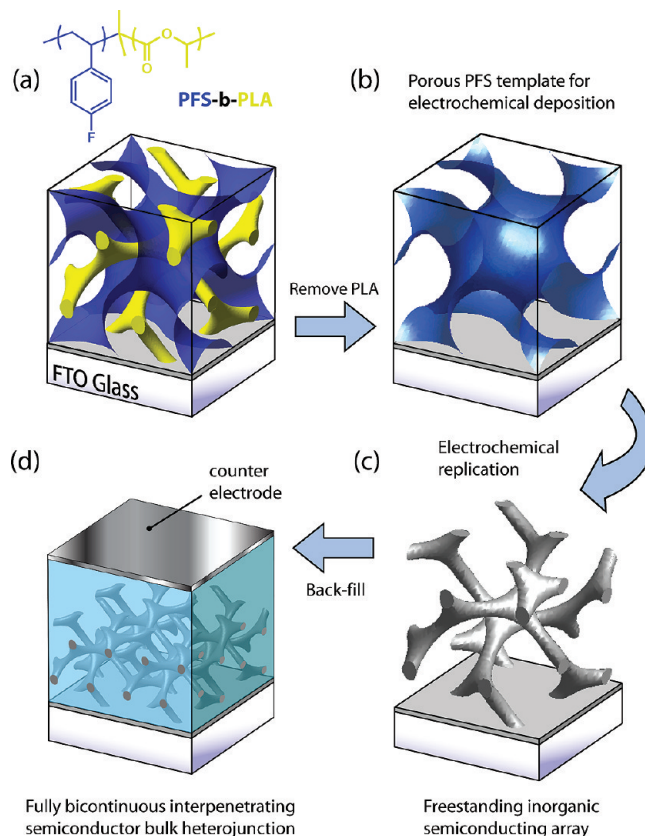
Figure 1. Schematic representation of gyroid network replication from block copolymer templates and assembly of hybrid solar cells. (a) PFS-b-PLA gyroid block copolymer morphology (for clarity only the representative central gyroid surface is shown for the majority PFS block). The polymer is prepared as a film on a glass substrate with transparent conducting oxide coating (FTO glass). (b) Voided PFS gyroid template after selective removal of the minority PLA networks. Electrochemical replication of the voided network proceeds uniformly from the underlying substrate. (c) Freestanding gyroid network array after removal of the supporting PFS template. (d) Back-filling of the array with a solid state hole transporting material and capping with a suitable counter electrode produces a bicontinuous bulk heterojunction solar cell architecture.

Panels a and b of Figure 2 show scanning electron micrographs (SEMs) of the free surface and cross section of such a bicontinuous polymer film. A magnified surface view is shown alongside a simulated [211] shallow projection of the gyroid phase with the gyroid networks removed (Figure 2, panels c and d). The unit cell size from these simulations was 47 ± 2 nm. Inspection of the films by SEM shows exclusively this characteristic double wave pattern at the free surface, suggesting preferential alignment of the (211) planes parallel to the substrate. Titanium(IV) oxide was deposited in the template via anodic oxidative hydrolysis of aqueous $TiCl_3$ in a standard three-electrode electrochemical cell. Panels e and f of[24] Figure 2 show a surface view of the replicated hydrated Ti(IV) oxide array after removal of the polymer template together with the simulated shallow [211] projection of the gyroid network phase. The high-magnification SEM examination confirms the near perfect replication of the gyroid template voids. The lower magnification SEM images in Figure 3 show that the array grows
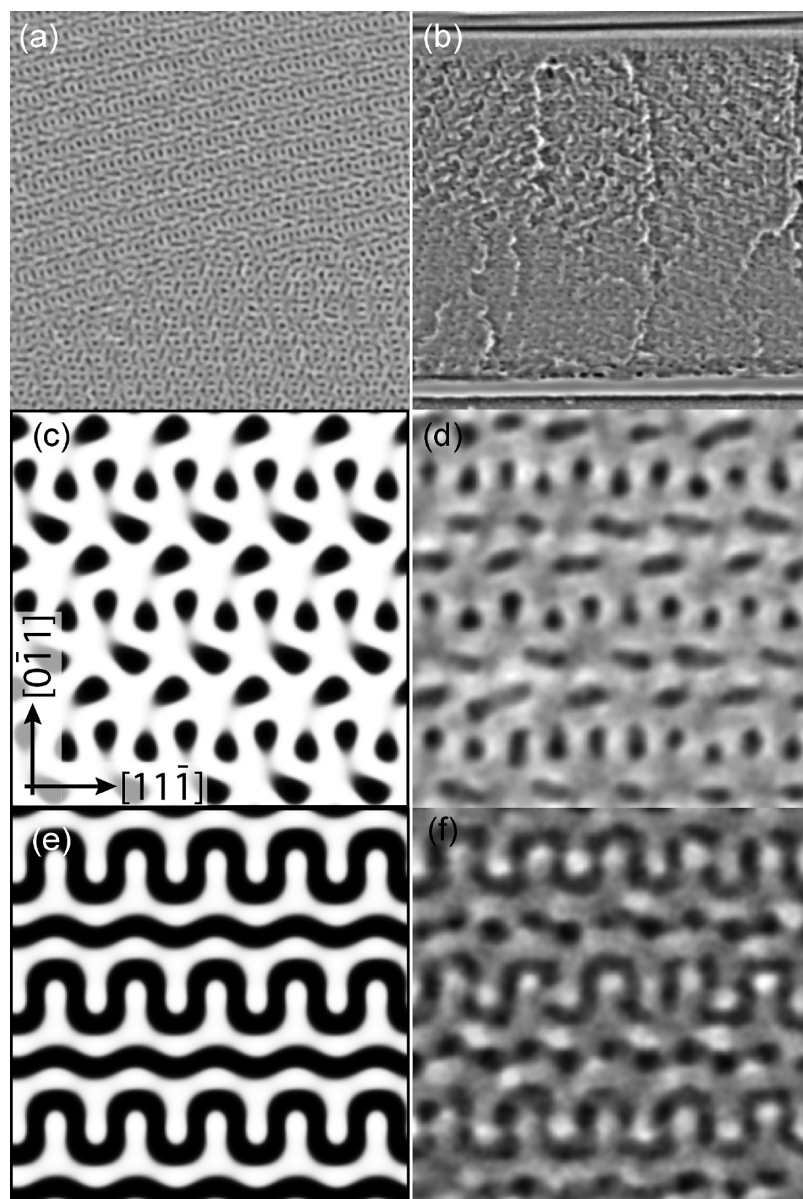
Figure 2. Gyroid-forming polymer templates and their electrochemical replication. (a) Surface and (b) cross-sectional SEM images of porous gyroid-forming films after selective removal of the minority PLA phase. Image sizes: 1 μm. (c) Magnified surface SEM from the template in (a), alongside a simulated [211] porous projection for a gyroid unit cell dimension of 47 nm (d). (e) Corresponding surface SEM image of a replicated Ti(IV) oxide nanostructure electrochemically deposited into the polymer template followed by dissolution of the polymer and comparison to the [211] simulated relief projection (f). Image sizes (c−f): 200 nm. The [211] projections were produced using Matlab and a level set approximation to the gyroid morphology.[34]

uniformly upward from the substrate into the polymer template, resulting in transparent and optically smooth films over large substrate areas (several cm²). The Ti(IV) oxide−PFS gyroid mesostructure was annealed on a hotplate at 500 °C for 2 h under argon followed by 1 h under oxygen. This resulted in complete degradation of the polymer template and the simultaneous crystallization of the deposited material. The film undergoes a significant thickness reduction during temperature processing (see Supporting Information).

Grazing incidence small-angle X-ray scattering (GISAXS) was used to study the order and orientation of the films over macroscopic length scales (centimeters) for the three processing steps. The assignments of the diffraction peaks of the network arrays were made on the basis of a structure

possessing $Ia\bar{3}d$ symmetry, whose (211) planes are oriented parallel to the substrate, consistent with the SEM observations and GISAXS experiments on gyroid structures reported in the literature.[21,25] For the mesoporous PFS film (Figure 4a), the best match was obtained for a structure with a unit cell of 50.5 nm with a uniaxial compression of 9% perpendicular to the substrate (Figure 4d). For the nanostructured hydrated Ti(IV) oxide−PFS films (Figure 4b), a unit cell of 50 nm and a uniaxial compression of 21% was found (Figure 4e). GISAXS patterns confirm that periodic ordering is preserved after TiO₂ crystallization, and scattering can be indexed to a cubic unit cell that has been compressed by 52% (Figure 4, panels c and f).
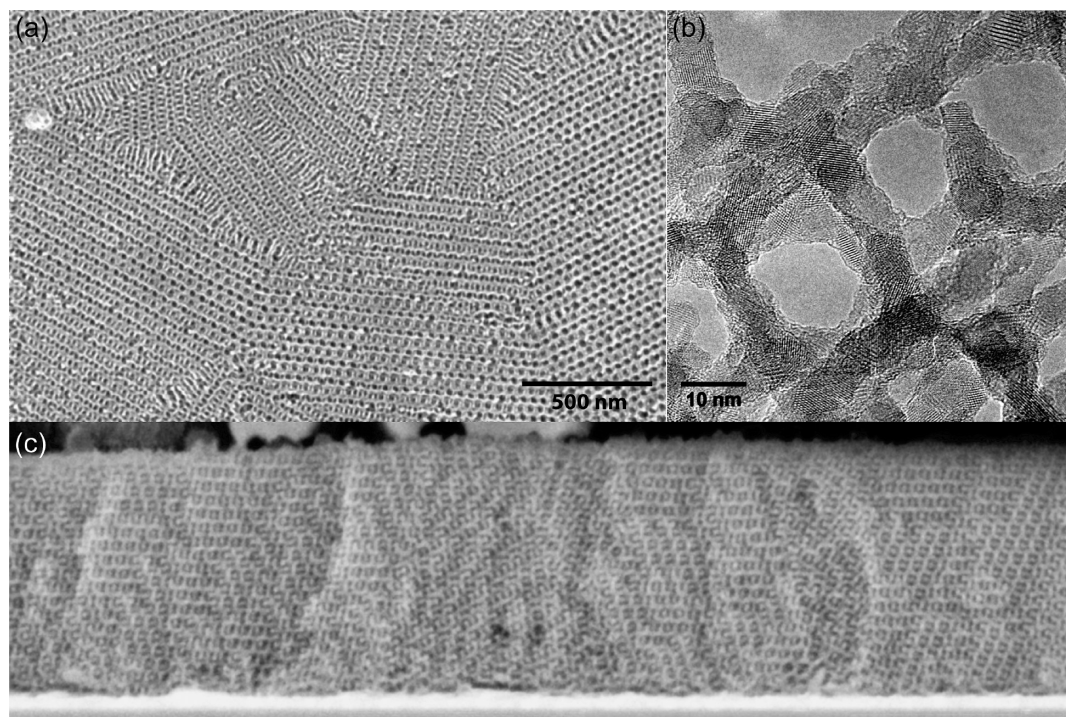
Figure 3. Electron microscopy characterization of freestanding bicontinuous gyroid semiconductor networks. (a) Surface SEM image of replicated anatase TiO_2 gyroid network after oxidative removal of the polymer template. (b) HRTEM image of the polycrystalline TiO_2 network composed of ~10 nm sized anatase grains. (c) Low-magnification cross-sectional SEM image of a Ti(IV) oxide array demonstrating the uniformity of the replication process (image width, 3 μm).
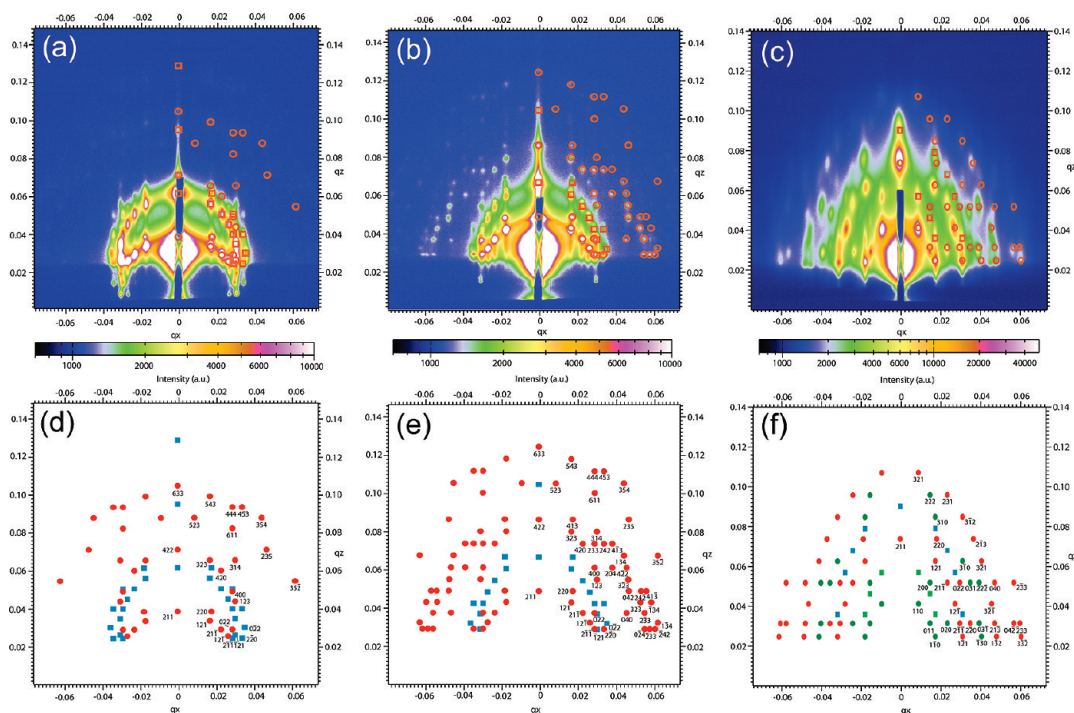

Figure 4. Experimental GISAXS pattern and indexation[35] of a voided PFS template after removal of minority component (a, d) nanostructured hydrated Ti(IV) oxide films with the PFS block still in place (b, e) and annealed titania network array (c, f). The patterns were analyzed using the distorted wave Born approximation to account for scattering of both the direct and reflected beam.[36,37] Red circles and blue boxes denote the diffraction peaks due to scattering of the direct and reflected X-ray beams, respectively. Green circles and green boxes indicate "forbidden" reflections. Only the diffraction peaks due to the direct beam scattering are indexed and only observed peaks are marked.

Grazing incidence wide-angle X-ray scattering (GIWAXS) patterns are consistent with nanocrystalline anatase TiO_2 with an average crystallite diameter of 9 nm, calculated by Debye−Scherrer peak width analysis (see Supporting Information). These assignments are supported by high-resolution transmission electron microscopy (HRTEM) studies (Figure
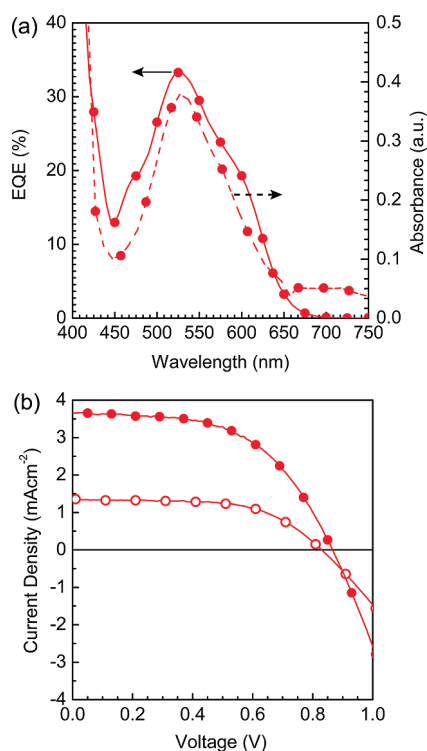
Figure 5. Solid-state-dye sensitized solar cell performance incorporating gyroid-patterned TiO$_2$ films. (a) External quantum efficiency, EQE (full lines), and absorption (dashed lines) for a solid-state dye-sensitized solar cell made using a 400 nm array sensitized with D149. The peak EQE value was 33%. (b) The current−voltage characteristics of 400 nm thick solid-state cells sensitized with Z907 (open circles) and D149 (solid circles) with power conversion efficiencies of 0.7% and 1.7%, respectively. The open-circuit voltages are 830 and 870 mV, the short-circuit currents are 1.35 and 3.66 mA cm^{-2}, and the fill factors are 0.60 and 0.54, for open circles and solid circles, respectively.

3b), showing polycrystalline gyroid network struts made up of anatase grains with sizes of the order of the strut diameter (∼10 nm). The uncompressed gyroid network has a calculated internal surface multiplicity of 125-fold per micrometer, consistent with the electrochemically active area of the same gyroid network replicated in platinum (see Supporting Information).

The performance of the TiO$_2$ gyroid arrays in photovoltaic devices was probed in a solid-state dye-sensitized solar cell. The titania was sensitized with either a standard bipyridyl ruthenium complex termed Z907[26] or a high extinction coefficient indoline dye termed D149,[27,28] and spiro-MeOTAD was infiltrated into the porous layer by spin-coating from a chlorobenzene solution containing Li-TFSI and *tert*-butylpyridine. A thermally evaporated Ag counter electrode completed the device. Figure 6a shows a SEM image of a cryo-fractured cross section of such a device and that of a similar film section before hole transporter infiltration (inset). Although it is difficult to quantify the degree of pore filling from SEM images,[29,30] it is clear that the majority of the pores are filled by spiro-MeOTAD, which appears dark in the SEM image.

The solid-state dye-sensitized solar cells incorporating ∼400 nm thick TiO$_2$ gyroid arrays sensitized with Z907 and D149 exhibit peak external quantum efficiencies (EQEs) of
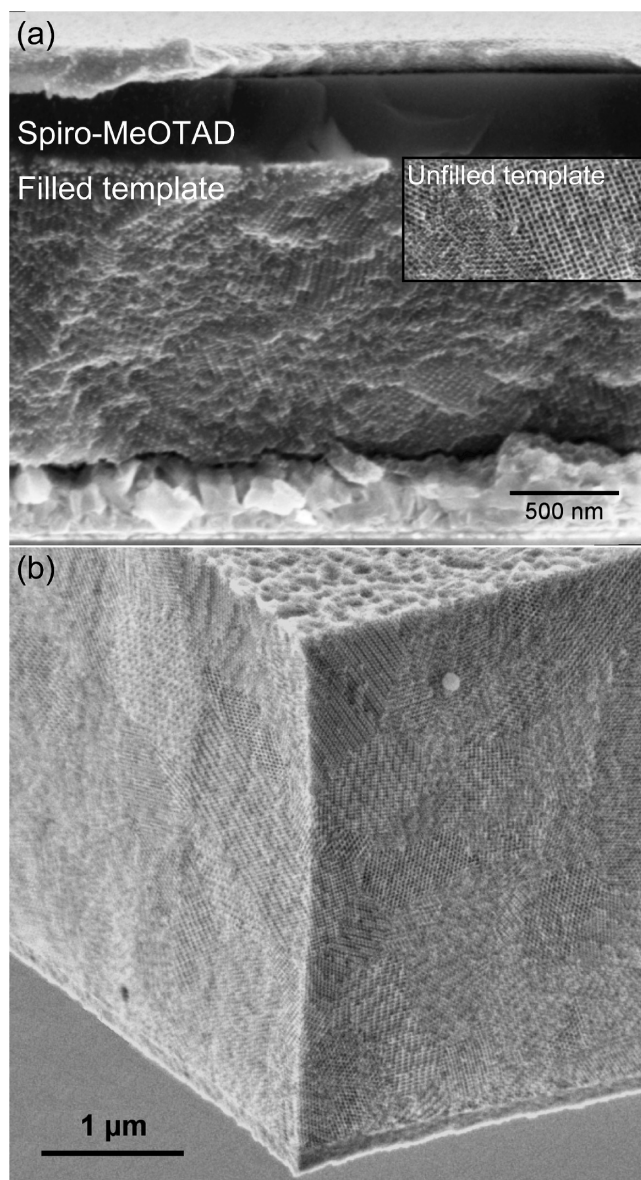

Figure 6. SEM fracture cross-section images of TiO$_2$ arrays. (a) 1.4 μm thick TiO$_2$ solid-state DSC cross section showing effective infiltration of spiro-MeOTAD (dark). (b) The ∼4 μm thick TiO$_2$ array demonstrates that the gyroid template remains fully porous in much thicker films, enabling deposition of thick arrays which grow uniformly upward from the underlying substrate.

14% and 33%, respectively (Figure 5a). Current−voltage characteristics measured under simulated AM 1.5 solar illumination of 100 mW cm^{-2} for the same devices are shown in Figure 5b, with overall power conversion efficiencies of 0.7% for Z907 sensitization and 1.7% using D149. We attribute the remarkable performance of the latter in such a thin film to both the high absorption strength of the D149 sensitizer and the excellent compatibility of the gyroid mesostructure with this class of solar cell: Random nanoparticle assemblies can lead to poorly controlled pore sizes and are likely to have partial domains that are predominantly disconnected from the continuous TiO$_2$ structure, resulting in highly torturous electron transport pathways.[31] For SDSCs, extremely small pores and dead ends are not easily filled by the bulky hole transporter. In contrast, the gyroid morphology

ensures that monodisperse channels and struts are all fully interconnected throughout the active layer.

While the power conversion efficiencies of the SDSCs in Figure 5 are lower in absolute terms compared to the record state-of-the-art in thick nanoparticle layers,[32] it is notable that the performance of our devices in this early stage of development is already directly competitive with fully optimized state-of-the-art nanoparticle-based SDSCs with comparable TiO_2 layer thicknesses.[2] A detailed characterization of the electronic properties of the gyroid morphology in comparison with nanoparticle and nanowire-based devices is reported in the following letter in this journal.[33]

The SEM image of a section of anatase gyroid array presented in Figure 6b shows that the formation of thicker, well-defined gyroid-patterned titania layers is feasible. It is a challenge, however, to manufacture SDSCs with these thicker layers because of the volume contraction of the titania during the annealing processing stage, causing stresses and failure at the substrate interface. Preliminary results indicate that it is possible to resolve this issue, and this is our current research challenge with this system. Finally, we emphasize that our method of using a copolymer gyroid morphology as a sacrificial template is quite general and may easily be adapted to manufacture hybrid solar cells based on different materials and bulk heterojunction all-organic solar cells and for other applications such as batteries, fuel cells, and catalysis where a large and controlled internal surface is required.

Note Added after ASAP Publication: Additions to the Acknowledgment were made to the version published November 13, 2008; the corrected version was reposted November 26, 2008.

Supporting Information Available: Further X-ray scattering, electron microscopy characterization, and electro-chemical surface area data. This material is available free of charge via the Internet at http://pubs.acs.org.

References

(1) Malliaras, G.; Friend, R. *Phys. Today* **2005**, *58*, 53–58.
(2) Snaith, H. J.; Schmidt-Mende, L. *Adv. Mater.* **2007**, *19*, 3187–3200.
(3) Gregg, B. A. *J. Phys. Chem. B* **2003**, *107*, 4688–4698.
(4) Yang, X.; Loos, J. *Macromolecules* **2007**, *40*, 1354–1362.
(5) Coakley, K. M.; McGehee, M. D. *Chem. Mater.* **2004**, *16*, 4533–4542.
(6) O'Regan, B.; Grätzel, M. *Nature* **1991**, *353*, 737–739.
(7) Bach, U.; Lupo, D.; Comte, P.; Moser, J. E.; Weissörtel, F.; Salbeck, J.; Spreitzer, H.; Grätzel, M. *Nature* **1998**, *395*, 583–585.
(8) Hamley, I. W. *The physics of block copolymers*; Oxford University Press: Oxford, 1998.
(9) Templin, M.; Franck, A.; Chesne, A. D.; Leist, H.; Zhang, Y.; Ulrich, R.; Schädler, V.; Wiesner, U. *Science* **1997**, *278*, 1795–1798.
(10) Zhao, D.; Feng, J.; Huo, Q.; Melosh, N.; Fredrickson, G. H.; Chmelka, B. F.; Stucky, G. D. *Science* **1998**, *279*, 548–552.
(11) Johnson, B. J. S.; Wolf, J. H.; Zalusky, A. S.; Hillmyer, M. A. *Chem. Mater.* **2004**, *16*, 2909–2917.
(12) Lin, Y.; Boker, A.; He, J.; Sill, J.; Xiang, H.; Abetz, C.; Li, X.; Wang, J.; Emrick, T.; Long, S.; Wang, Q.; Balazs, A.; Russell, T. P. *Nature* **2005**, *434*, 55–59.
(13) Warren, S. C.; Disalvo, F. J.; Wiesner, U. *Nat. Mater.* **2007**, *6*, 156–161.
(14) Coakley, K. M.; Liu, Y.; McGehee, M. D.; Frindell, K. L.; Stucky, G. D. *Adv. Funct. Mater.* **2003**, *13*, 301–306.
(15) Zukalová, M.; Zukal, A.; Kavan, L.; Nazeeruddin, M. K.; Liska, P.; Grätzel, M. *Nano Lett.* **2005**, *5*, 1789–1792.
(16) Hajduk, D. A.; Harper, P. E.; Gruner, S. M.; Honeker, C. C.; Kim, G.; Thomas, E. L.; Fetters, L. J. *Macromolecules* **1994**, *27*, 4063–4075.
(17) Schulz, M. F.; Bates, F. S.; Almdal, K.; Mortensen, K. *Phys. Rev. Lett.* **1994**, *73*, 86–89.
(18) Mao, H.; Hillmyer, M. A. *Soft Matter* **2006**, *2*, 57–59.
(19) Hashimoto, T.; Nishikawa, Y.; Tsutsumi, K. *Macromolecules* **2007**, *40*, 1066–1072.
(20) Armatas, G. S.; Kanatzidis, M. G. *Nature* **2006**, *441*, 1122–1125.
(21) Urade, V. N.; Wei, T.; Tate, M. P.; Kowalski, J. D.; Hillhouse, H. W. *Chem. Mater.* **2007**, *19*, 768–777.
(22) Cho, B. K.; Jain, A.; Gruner, S. M.; Wiesner, U. *Science* **2004**, *305*, 1598–1601.
(23) Crossland, E. J. W.; Ludwigs, S.; Hillmyer, M. A.; U.Steiner, *Soft Matter* **2007**, *3*, 94–98.
(24) Kavan, L.; O'Regan, B.; Kay, A.; Grätzel, M. *J. Electroanal. Chem.* **1993**, *346*, 291–307.
(25) Lee, B.; Park, I.; Yoon, J.; Park, S.; Kim, J.; Kim, K. W.; Chang, T.; Ree, M. *Macromolecules* **2005**, *38*, 4311–4323.
(26) Schmidt-Mende, L.; Zakeeruddin, S.; Grätzel, M. *Appl. Phys. Lett.* **2005**, *86*, 013504.
(27) Horiuchi, T.; Miura, H.; Sumioka, K.; Uchida, S. *J. Am. Chem. Soc.* **2004**, *126*, 12218–12219.
(28) Howie, W. H.; Claeyssens, F.; Miura, H.; Peter, L. M. *J. Am. Chem. Soc.* **2008**, 1367–1375.
(29) Schmidt-Mende, L.; Grätzel, M. *Thin Solid Films* **2006**, *500*, 296–301.
(30) Snaith, H. J.; Humphry-Baker, R.; Chen, P.; Cesar, I.; Zakeeruddin, S. M.; Grätzel, M. *Nanotechnology* **2008**, *19*, 424003.
(31) Benkstein, K. D.; Kopidakis, N.; van de Lagemaat, J.; Frank, A. J. *J. Phys. Chem. B* **2003**, *107*, 7759–7767.
(32) Snaith, H. J.; Moule, A. J.; Klein, C.; Meerholz, K.; Friend, R. H.; Grätzel, M. *Nano Lett.* **2007**, *7*, 3272–3276.
(33) Crossland, E. J. W.; Nedelcu, M.; Ducati, C.; Ludwigs, S.; Hillmyer, M. A.; Steiner, U. *Nano Lett.* **2009**, *9*, 2813–2819.
(34) The scientific graphics project: http://www.msri.org/about/sgp/SGP/index.html′.
(35) Smilgies, D. M.; Blasini, D. R. *J. Appl. Crystallogr.* **2007**, *40*, 716–718.
(36) Busch, P.; Rauscher, M.; Smilgies, D.-M.; Posselt, D.; Papadakis, C. M. *J. Appl. Crystallogr.* **2006**, *39*, 433–442.
(37) Rauscher, M.; Salditt, T.; Spohn, H *Phys. Rev. B* **1995**, *52*, 16855–16863.

NL803174P

Supporting Online Material for

A bicontinuous double gyroid hybrid solar cell

Edward J.W. Crossland[1,2], Marleen Kamperman[3], Mihaela Nedelcu[1], Caterina Ducati[4], Ulrich Wiesner[3], Detlef -M. Smilgies[5], Gilman E.S. Toombes[6], Marc A. Hillmyer[7], Sabine Ludwigs[1,8], Ullrich Steiner[*1] & Henry J. Snaith[*9]

[1]Department of Physics, Cavendish Laboratory, University of Cambridge, Cambridge CB3 0HE, UK, and University of Cambridge Nanoscience Centre, Cambridge, CB3 0FF, UK

[2]Freiburg Institute for Advanced Studies, Albert-Ludwigs-Universität Freiburg, 79104 Freiburg, Germany

[3]Department of Materials Science & Engineering, Cornell University, Ithaca, New York 14853, USA

[4]Department of Materials Science & Metallurgy, University of Cambridge, Cambridge, CB2 3QZ, UK

[5]Cornell High energy Synchrotron Source (CHESS), Cornell University, Ithaca, New York 14853, USA

[6]Physical Chemistry - UMR CNRS 168, Institute Curie, 11 rue Pierre et Marie Curie, 75005 Paris, France

[7]Department of Chemistry, University of Minnesota, Minneapolis, MN 55455-0431, USA

[8]Institute for Macromolecular Chemistry & Freiburg Materials Research Centre, University of Freiburg, Stefan-Meier-Str. 31, 79104 Freiburg, Germany

[9]Clarendon Laboratory, Department of Physics, University of Oxford, OX1 3PU, UK

[*]e-mail: u.steiner@bss.phy.cam.ac.uk and h.snaith1@physics.ox.ac.uk

Materials and Methods

Substrate and polymer template preparation

FTO glass substrates (Nippon Glass) were cleaned with acetone, isopropanol and exposure to O_2 plasma for 5 minutes and coated with a compact TiO_2 film ($\sim$ 70 nm) by spray-pyrolysis deposition as previously described.[1,2] PFS-PLA films with thicknesses of up to $1\,\mu$m were spin-cast from 10 % toluene solutions onto these substrates. Thicker films (up to $10\,\mu$m) were formed via doctor-blade coating of the same solution over strips of the prepared substrates. The films were annealed at $180\,^\circ$C in a N_2 atmosphere for 35 h and allowed to cool to room temperature over 3 hours. The PLA component was selectively removed by immersing the films in 0.05 M $NaOH_{(aq)}$ containing 40 %$_{vol}$ MeOH at room temperature for several hours.[3] The etching rate of PLA is approximately $1\,\mathrm{nm\,s}^{-1}$ under these conditions.[4]

Electrochemical deposition of Titania

Electrochemical synthesis of hydrated Ti(IV) oxide mesostructured films was performed from 0.2 M aqueous $TiCl_3$ at pH 2.7, containing 20 % methanol (Laboratory reagent grade $\geq$ 99.5 %). The electrolyte was prepared from $\sim$10 %$_{mass}$ Titanium (III) Chloride in HCl (Sigma-Aldrich) by drop-wise addition of a 20 %$_{mass}$ Na_2CO_3 solution. All solutions were continuously purged with nitrogen during preparation and electrochemical deposition at room temperature. The working electrode (anode) was held at 0 V vs Ag/AgCl in a standard three-electrode cell with a platinum wire counter electrode using a CH Instruments potentiostat. The filled templates were annealed on a hotplate at $500\,^\circ$C for 2 hours under nitrogen, then for a further hour in an oxygen flow in order to form nanocrystalline TiO_2 and to completely burn away the polymer template. The resulting films were transparent and optically smooth.

Material and morphological characterization

The block copolymer and electrodeposited nanostructures were characterized by scanning electron microscopy (SEM) using a FEI Philips XL30 sFEG at an accelerating voltage of 5 kV with no additional coating. Cross-sectional images were obtained by immersing the sample in liquid nitrogen and fracturing the substrate. Specimens for high resolution transmission electron microscopy (HRTEM) were prepared by scraping material from the substrate onto a Cu TEM grid. The samples were examined using a Jeol 4000EX microscope, with 400 kV acceleration voltage and a point resolution of 0.17 nm.

Grazing Incidence Small Angle X-ray Scattering (GISAXS)

Scattering experiments were performed at the G1 line at Cornell High Energy Synchrotron Source (CHESS). Data were collected with a CCD 2-D detector. The operating conditions are given in Table 1. The GISAXS patterns were calculated using Matlab, following the index scheme described earlier.[5] The predicted patterns were overlaid on the experimental data and the cubic unit cell and the degree of uniaxial compression were varied until the best match was obtained. GISAXS patterns were analyzed using the distorted wave Born approximation to account for scattering of the direct and reflected beam. The assignments of the diffraction peaks were made on the basis of a structure possessing Ia$\bar{3}$d symmetry, whose (211) planes are oriented parallel to the substrate, consistent with SEM observations and GISAXS experiments on gyroid structures reported in the literature.[6,7] The unlabeled peaks in the range $0 < qz < 0.02$ are probably transmission peaks through the edges of the sample, since they appear below the critical angle of the film. Upon TiO_2 crystallization the film undergoes a large compression in the direction normal to the substrate.

2

Compression of a cubic lattice breaks some of the symmetries of the Ia$\bar{3}$d space-group and forbidden 110, 200, 310, and 222 reflections are observed.[6,8] The relatively high intensity of the 110 compared to the 211 reflections might be caused by a shift of the two nanowire networks relative to each other.[9] Another mechanism leading to bright 110 reflections arises if only one of the two distinct networks of the double-gyroid survives the calcination process in parts of the sample.

Solid-state dye-sensitized solar cell construction

Solid-state dye-sensitized solar cells were fabricated by cooling the TiCl$_4$ treated and annealed TiO$_2$ films to 70 °C followed by immersion in a 0.5 mM solution of a ruthenium complex sensitizer, termed Z907, overnight, or in a 0.5 mM solution of an indolene dye, termed D149, for 10 minutes. The dyed films were rinsed in acetonitrile and coated with 15 μl of Spiro-MeOTAD solution (100 μl chlorobenzene, 18 mg Spiro-MeOTAD, 1.75 μl of tertial-butyl pyridine and 3.75 μl of Lithium-TFSI ACN solution (170 mg/ml)) for 40 s before spin-coating at 2000 rpm for 30 seconds.[10] The coated films were then capped with 200 nm thick silver electrodes via thermal evaporation under high vacuum.

Device testing

To determine the spectral response of the photocurrent, a halogen lamp (spectrally resolved by a monochromator) illuminated the solar cells from the FTO side, at an intensity of order 0.1 mWcm^{-2} at each wavelength interval. The illumination spot size was approximately 1 mm^2, and the photocurrent was measured by a Keithley 237 source meter interfaced with a computer. The spectral dependence of the power incident on the devices was calibrated with a reference Si photodiode. The simulated AM 1.5 solar illumination was generated by a 300 W Oriel solar simulator with the corresponding AM 0 and AM 1.5 filters. The intensity of the solar simulator was calibrated using a Si calibration diode purchased from and calibrated at the Fraunhofer Institute for Solar Energy System. The spectral mismatch was calculated over the entire absorbing region of the test cell and calibration diode following the method of Seaman.[11] The active area of the SDSCs was defined to be approximately 0.045 cm^2 by the overlap of the silver cathode with the FTO anode. Using an optical mask for the solid-state devices made negligible difference to the measured photocurrent.

References

1. Kavan, L.; Grätzel, M. *Electrochim. Acta* **1995,** *40,* 643-652.

2. Snaith, H. J.; Grätzel, M. *Adv. Mater* **2006,** *18,* 1910-1914.

3. Zalusky, A. S.; R.Olayo-Valles,; Wolf, J. H.; Hillmyer, M. A. *J. Am. Chem. Soc.* **2002,** *124,* 12761-12773.

4. Crossland, E. J. W.; Cunha, P. M. S.; Ludwigs, S.; Hillmyer, M. A.; Steiner, U. **2008,** (In Preparation).

5. Smilgies, D. M.; Blasini, D. R. *J. Appl. Cryst.* **2007,** *40,* 716-718.

6. Urade, V. N.; Wei, T.; Tate, M. P.; Kowalski, J. D.; Hillhouse, H. W. *Chem. Mater.* **2007,** *19,* 768-777.

7. Lee, B.; Park, I.; Yoon, J.; Park, S.; Kim, J.; Kim, K. W.; Chang, T.; Ree, M. *Macromol.* **2005,** *38,* 4311-4323.

8. Toombes, G. E. S.; Finnefrock, A. C.; Tate, M. W.; Ulrich, R.; Wiesner, U.; Gruner, S. M. *Macromolecules* **2007,** *40,* 8974-8982.

9. Solovyov, L. A.; Zaikovskii, V. I.; Shmakov, A. N.; Belousov, O. V.; Ryoo, R. *J. Phys. Chem. B* **2002,** *106,* 12198-12202.

10. Snaith, H. J.; Schmidt-Mende, L.; Grätzel, M. *Phys. Rev. B.* **2006,** *74,* 045306.

11. Seaman, C. *Solar Energy* **1982,** *29,* 291-298.

12. Trasatti, S.; Petrii, O. A. *J. Electroanal. Chem.* **1992,** *327,* 353-376.

13. Luzzati, V.; Spegt, P. A. *Nature* **1967,** *215,* 701.

Supplementary Table and Figures

Supplementary Table 1. X-ray operating conditions.

Supplementary Figure 1. Small angle X-ray scattering (SAXS) pattern for a bulk sample of PFS-*b*-PLA annealed at $180\,^\circ$C. Peaks with scattering wave vector $q = 4\pi \sin(\theta)/\lambda$ spacing-ratios of $\sqrt{6}$, $\sqrt{8}$, $\sqrt{14}$, $\sqrt{16}$, $\sqrt{20}$, $\sqrt{22}$, $\sqrt{30}$, $\sqrt{32}$, $\sqrt{38}$, $\sqrt{40}$, $\sqrt{42}$, $\sqrt{46}$, $\sqrt{48}$, $\sqrt{50}$ are discernible, consistent with a gyroid phase with a unit cell of 49 nm. The expected peaks for an Ia$\bar{3}$d cubic lattice are indicated by vertical lines. Bulk samples of the polymer were annealed under vacuum for 70 h at $180\,^\circ$C and cooled to room temperature at $\sim 10\,^\circ$C/min. The structure is frozen-in by cooling the sample below the glass transition temperature of the two phases ($103\,^\circ$C for PFS and $57\,^\circ$C for PLA).

Supplementary Figure 2. Real-space observation of gyroid array contraction during annealing. (a) Cross-sectional SEM image of the electrochemically replicated Ti(IV) oxide network in the PFS template before temperature treatment. (b) Cross-section of the same film after annealing for 2 h at $500\,^\circ$C. (d) is an enlarged view of (a) after rinsing away the PFS template in an organic solvent and (e) is an enlarged view of (b) showing the strong compression of the TiO_2 anatase network during annealing (image size: 200 nm). The image in (f) shows a version of (e) that was digitally expanded in the vertical direction to match the simulated (011) gyroid plane projection in (c). This visualizes the strong compression the sample undergoes during annealing, which reflects the reduction in film thickness moving from (a) to (b).

Supplementary Figure 3. Grazing incidence wide-angle X-ray diffraction scattering (GIWAXS) of a titania array after annealing at $500\,^\circ$C. The peaks are consistent with nanocrystalline anatase TiO_2 with an average crystallite diameter of 9 nm calculated by a Debye-Scherrer peak width analysis after correction for peak width resolution ($\Delta(2\theta) = \sqrt{\Delta(2\theta)^2_{meas} - \Delta(2\theta)^2_{res}}$ with $\theta_{res} = 0.18^\circ$). The data were collected at a X-ray wavelength of 1.21 Å. The powder spectra were calibrated by comparison to simulated spectra of cassiterite using the crystal structure visualization program "Mercury" (Cambridge Crystallographic Data Centre).

Supplementary Figure 4. Electrochemical measurement of the gyroid surface area. A 300 nm thick platinum gyroid network was replicated by potentiostatic electrochemical deposition at +0.1 V vs. Ag/AgCl from an aqueous solution of 20 mM H_2PtCl_6 containing 20 $\%_{vol}$ methanol. The polymer template was removed by rinsing in toluene. The surface area of the Pt network was determined by measuring the charge associated with hydrogen adsorption in a 0.1 M $H_2SO_{4\,(aq)}$ solution with a potential scan rate of 50 mV s^{-1} and a conversion factor of $210\,\mu$C cm^{-2}.[12] The array was first subjected to an electrochemical cleaning procedure involving oxygen and hydrogen evolution to clean the Pt surface. The measured charge H_C was 8.01 mC cm^{-2} which translates to a surface multiplicity in electrochemically accessible area of 130 fold per μm of array thickness. Using a simple cylindrical channel model[13], the surface area of an uncompressed voided gyroid template ($S = 7.297\pi d/a^2 f_{PFS}\rho_{PFS}$) is 208 m^{2}g^{-1} (using pore size $d = 12$ nm, unit cell $a = 47$ nm, PFS density $\rho_{PFS} = 1$ g cm^{-3} and volume fraction $f_{PFS} = 0.6$). Assuming the replicated structure has the same total surface as the template and neglecting sub-10 nm surface roughness, this predicts a surface multiplicity of 125 fold per micron for the templated gyroid network array.

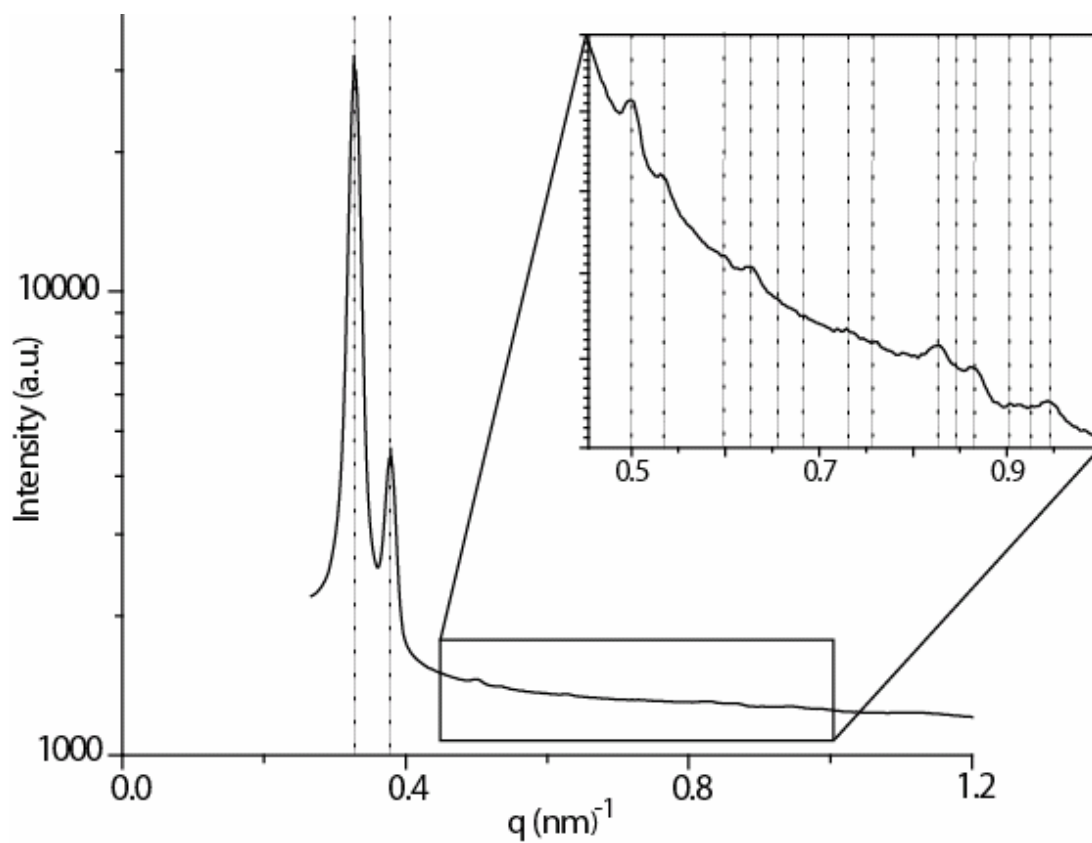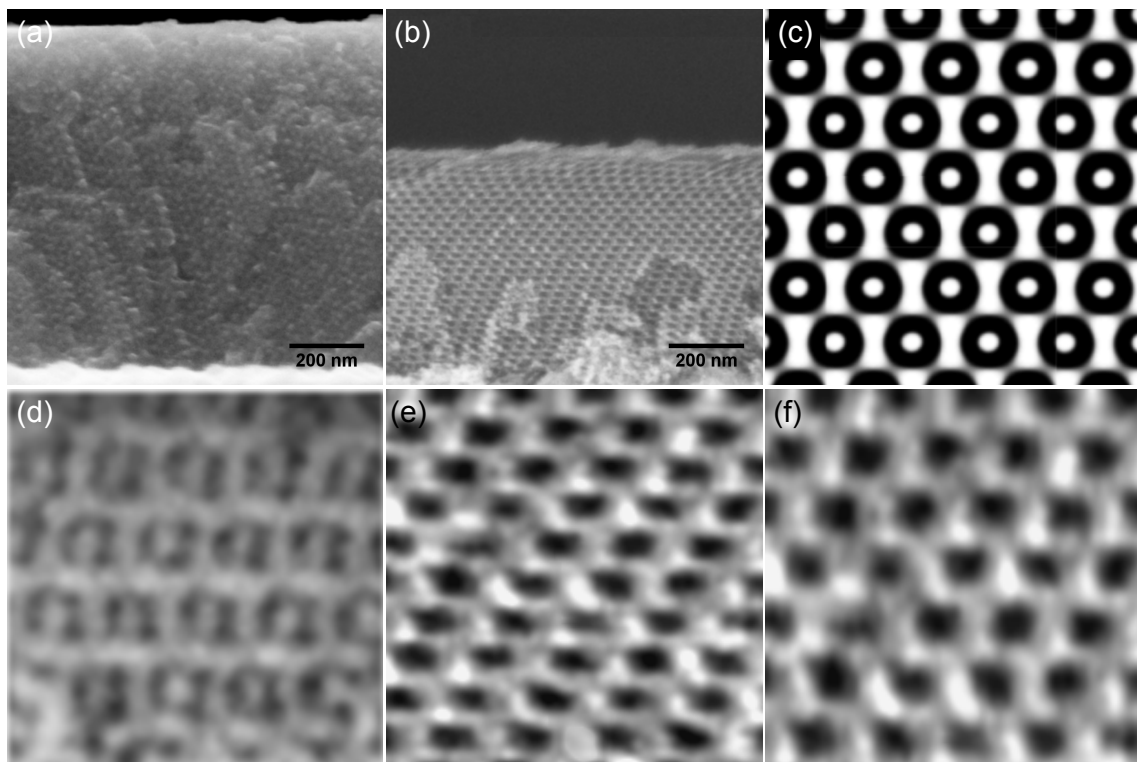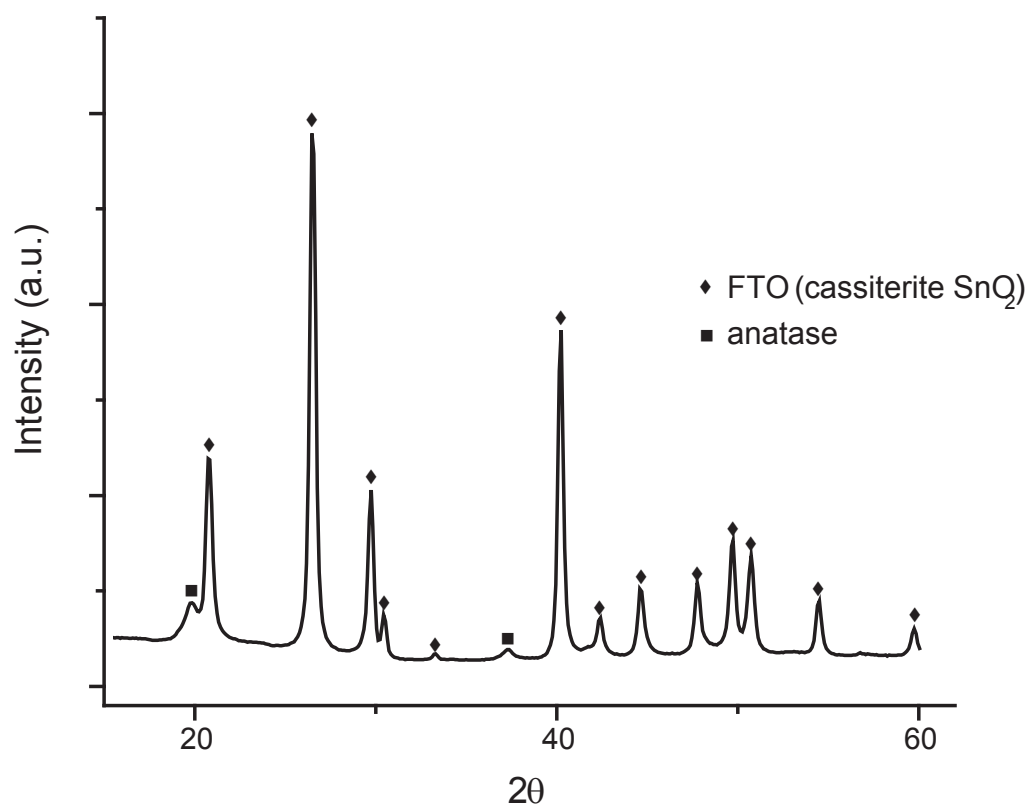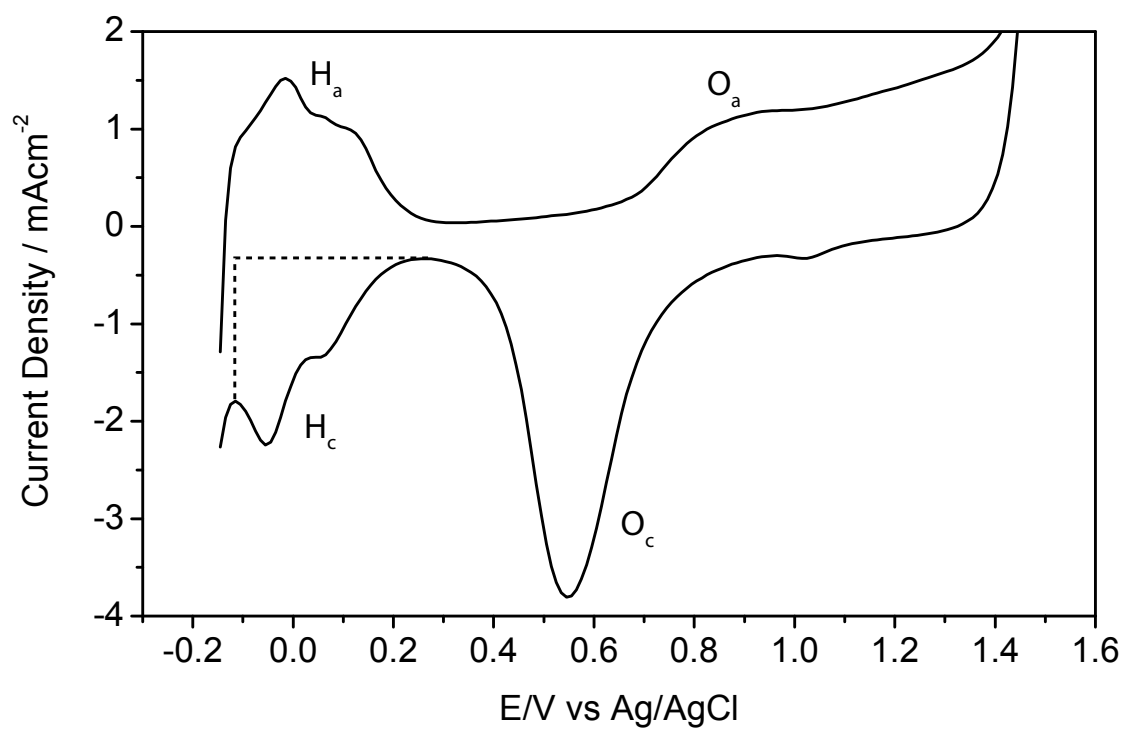|	X-ray energy (Å)	Sample-detector distance (mm)	Exposure time (s)	Incident angle α_{inc} (°)
Bulk PFS-*b*-PLA	1.538	1319	3.00	-
Voided PFS template	1.223	1920	0.02	0.18
Hydrated Ti(IV) oxide films	1.223	1920	0.10	0.18
Calcined mesoporous titania	1.538	1936	0.20	0.19

Table 1:

Figure 1:

Figure 2:

Figure 3:

Figure 4: